Egypt. J. Geo. **Vol. 68,** pp: 437 - 450 (2024)

Egyptian Journal of Geology

https://egjg.journals.ekb.eg

Petrophysical Studies for Shaly Sand Reservoirs in Saffron Field, Nile Delta, Egypt

Osama S. Moselhy [1], Abdel Moktader A. El Sayed [2] and **Amir M. Lala [2]**

[1] *Rashid Petroleum Company, Cairo, Egypt*
[2] *Geophysics Department, Faculty of Science, Ain Shams University, Cairo, Egypt*

Saffron Gas Field, situated within the West Delta Deep Marine (WDDM) concession on the north-western margin of the Nile Delta. The hydrocarbons in this field are extracted from the Saffron sand reservoirs. Many wells have been drilled and have penetrated these reservoirs. The petrophysical evaluation, conducted using well-log data, aims to identify hydrocarbon-bearing reservoirs and examine reservoir properties based on data from four wells. This study utilizes the Tech-log Schlumberger software packages for its analyses.

The four wells provided ample data for detailed analysis, allowing evaluation of some petrophysical parameters such as shale volume (Vsh), total porosity (PHT), effective porosity (PHE), water saturation (Sw), hydrocarbon saturation (Sh), and net-to-gross reservoir thickness. Both conventional log tools and advanced CMR tools (Combinable magnetic resonance) were used in the present study, with a comparison between traditional and advanced techniques.

Keywords: Petrophysical Evaluation, Porosity, Permeability, Saturation, Lithology, Density, Neutron and CMR logs, Saffron Gas Field. WDDM (West Delta Deep Marine).

1. Introduction

The Nile Delta is considered as gas-producing region with substantial reserves in its deep-water areas. Spanning approximately 50,000 km², the modern Nile Delta's area is evenly distributed between onshore and offshore regions. The offshore, Saffron Field, is a part of the West Delta Deep Marine concession. It contains multiple reservoirs within the Pliocene sandstones of the El Wastani Formation. The present study aims to provide a comprehensive geological and petrophysical analysis of the Saffron Field to enhance understanding of its hydrocarbon potentiality. The field features a stacked channel system with six distinct reservoirs, categorized as Channels A North, B, C, and E, collectively referred to as the Saffron North Complex, and two separate reservoirs, the A South Channel and Channel 11. (Figs.1, 2&3).

The Saffron reservoirs are situated within the Pliocene sandstones of the El Wastani Formation, interpreted as deep-water canyon fill deposits. These reservoirs comprise a heterogeneous succession of sandstones and mudstones, arranged in a broadly upward-fining sequence. The lower part of the section is dominated by high-quality, blocky sands, while the upper section features isolated sand bodies encased in thin-bedded sands and mudstones.

2. Data and Methods

2.1 Data Availability

Four wells were selected to investigate the Saffron Field reservoirs and assess the hydrocarbon potentiality in the study area. The open-hole log data, including conventional tools such as Gamma Ray, resistivity, calliper, sonic, neutron, and density logs, and advanced tools like CMR logs, were collected and digitized for the units studied.

The study employed both qualitative and quantitative analyses using the Techlog-v.2019 Schlumberger software. Cross-plots were utilized to illustrate the lithological and mineralogical components of the Saffron reservoirs. The shale content (Vsh) was calculated from gamma-ray and neutron-density logs. The minimum shale content indicated by these shale indicators is likely close to the actual Vsh value.

*Corresponding Author: geo_osamasaid@yahoo.com
Received: 07/12/2024; Accepted: 15/12/2024
DOI: 10.21608/EGJG.2024.342541.1096
©2024 National Information and Documentation Center (NIDOC)

Corrected porosity was estimated using a combination of the density and neutron logs after applying various corrections. Water saturation (Sw) was computed using the Indonesian equation for conventional evaluation. For advanced evaluation, CMR logs were used to estimate Vsh, total porosity, and effective porosity after correction with the density log. CMR logs also facilitated the estimation of water saturation and permeability.

2.2 Determination of Lithology from Wire Line Logs

A systematic computer-based interpretation of the lithology for the studied wells was conducted using all the registered logs. The initial step involved corroborating and comparing the gross lithology horizontally to the gamma-ray log at the same depth. This interpretation process then extended horizontally through other logs, including resistivity, sonic, density-neutron, and CMR logs, ensuring a comprehensive analysis of the lithological characteristics.

2.3 Estimation of Petrophysical Parameters

Listings of the various reservoir parameters by depth were also generated during the study.

2.3.1 Shale and Clay Volume

For the estimation of the Volume of shale from conventional tools, the minimum of gamma-ray was used to compute Vsh, as shown in equation 1(Schlumberger, 1972).

$$Vsh = \frac{GR\log - GRmin}{GR\ max - GR\ min} \quad (\mathbf{1})$$

Where:
Vsh= Volume of Clay
GR log= GR Log reading of formation
GR min= GR Matrix (Clay free zone)
GR max= GR Shale (100% Clay zone)

Estimation Vsh from CMR logs we used (Freedman, 1997)

$$Vsh = \frac{CBF2\log - CBF2\ min}{CBF2\ max - CBF2\ min} \quad (\mathbf{2})$$

Where:
CBF2= Porosity of clay bound water
CBF2 log= CBF2 reading of formation
CBF2 min= CBF2 (Clay free zone)
CBF2 max= CBF2 (100% Clay zone)

2.3.2 Porosity

Total porosity was calculated from the density-neutron log as shown in the following relationship, Asquith, G.B. and Gibson, C., (1982):

$$\varphi_t = \sqrt{\frac{\varphi_N + \varphi_D}{2}} \quad (\mathbf{3})$$

Where:
φ t= Porosity derived from density log
φ N =Neutron porosity read on log
φ D= density porosity (measured by this equation {(ρma – ρb)/ (ρma – ρfl)})

Effective porosity was estimated according to the following equation (Schlumberger, 1972)

$$\varphi_{eff} = \varphi_t - (\varphi_{sh} V_{sh}) \quad (\mathbf{4})$$

Where:
φ eff = Effective porosity
Vsh = Volume of shale
φ sh=porosity of shale

Porosity from CMR tool (Freedman, 1997) (Fig.4)

$$DMRP = 0.6 * DPHI + 0.4 * TCMR \quad (\mathbf{5})$$

Where:
DMRP= Total CMR porosity corrected
TCMR= Total CMR porosity
DPHI= Total Density porosity

Effective corrected porosity from CMR (Freedman, 1997)

$$DMRP.eff = DMRP - CBF2 \quad (\mathbf{6})$$

Where:
DMRP.eff= Effective CMR porosity corrected
DMRP= Total CMR porosity corrected
CBF2= Porosity of clay bound water

2.3.3 Water Saturation

Water saturation was estimated using the following Indonesian equation. (Schlumberger, 1972)

$$\frac{1}{\sqrt{R_d}} = \left[\frac{V_{sh}^{(1-0.5V_{sh})}}{\sqrt{R_{sh}}} + \frac{\left(\sqrt{\varphi_t}\right)^m}{\left(\sqrt{aR_w}\right)}\right]\left(\sqrt{S_w}\right)^n \quad (\mathbf{7})$$

Where,
Rd= Deep Resistivity
Rsh= resistivity in clay (read from log)
Rw= Down hole water resistivity
m= cementation factor
n= Saturation exponent, it is the gradient defined on the plot.

Water saturation from the CMR tool, (Freedman, 1997)

$$SWE = \frac{CW}{DMRPeff} \quad (\mathbf{8})$$

Where:
CW= capillary water.
DMRP.eff= Effective corrected porosity from CMR

2.3.4 Permeability from the CMR tool

We used a Timur-Coats model (Timur, A. 1969) to estimate the permeability from CMR logs.

$$KTC = a.\phi 4\,(FFV\ /\ BVF\ )2 \quad (9)$$

Where:

Porosity (ϕ) = Total CMR porosity corrected

FFV= Free Fluid Volume

BFV= Bound Fluid Volume

2.3.5 Net Pay

A porosity cut-off of 10% was used along with a shale volume cut-off of 60% to define the quality of the reservoir rock. Water saturation, Sw, a cut-off value of 70% was used to determine pay. The reservoirs were represented by a porosity greater than 10% and shale volume less than 60%. For the net pay, if the water saturation within the reservoir is less than 70%, it is considered to contain hydrocarbon.

2.3.6 Cross-Plots

In this study, two types of well-log cross-plots between two variables were done and the resulting series of points were used to define the relationships between the variables. The cross-plots include:

I. Cross-plots of compatible logs measure the same parameters as the porosity logs, neutron-density cross-plot.

II. Clay Minerals Identification using Natural Gamma Ray Spectrometry Tool (NGS).

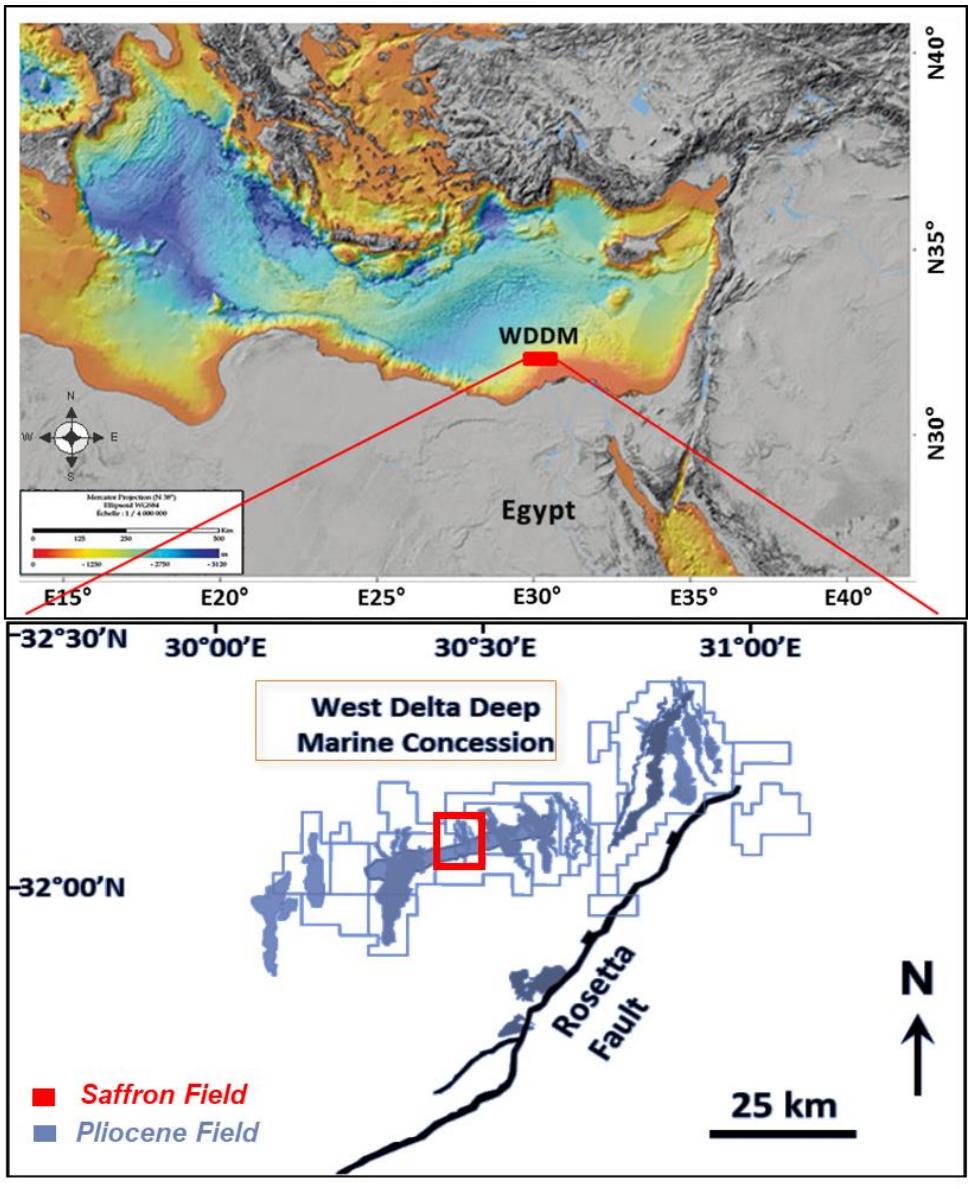

Fig. 1. Saffron field location map.

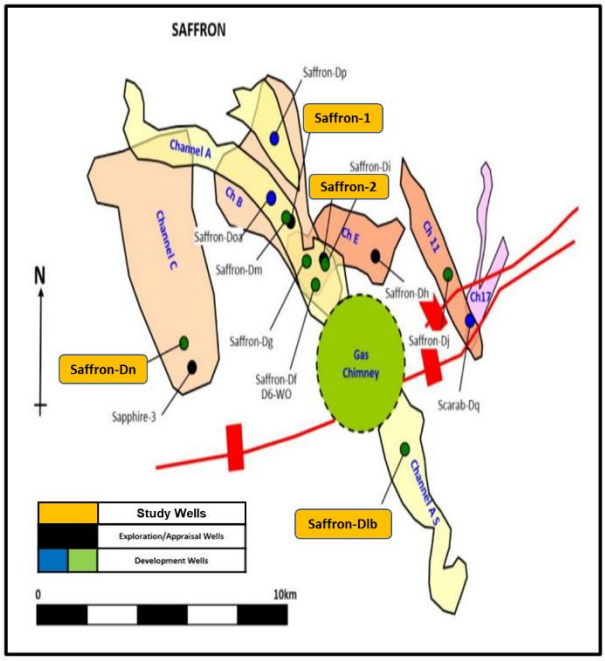

Fig. 2. A schematic map showing the field components

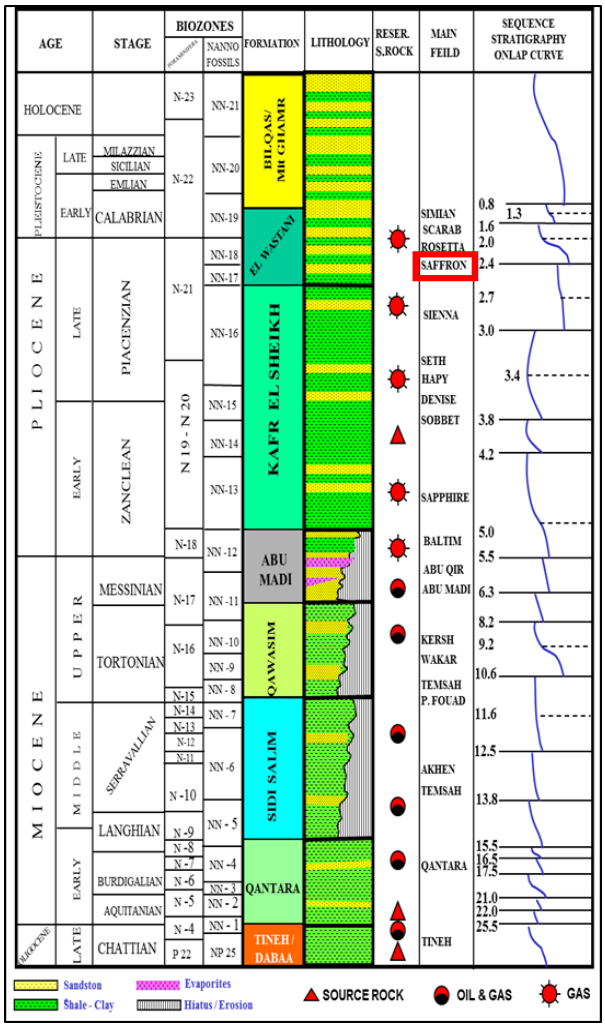

Fig. 3. Stratigraphic column of WDDM Nile Delta (Cross, et al., 2009).

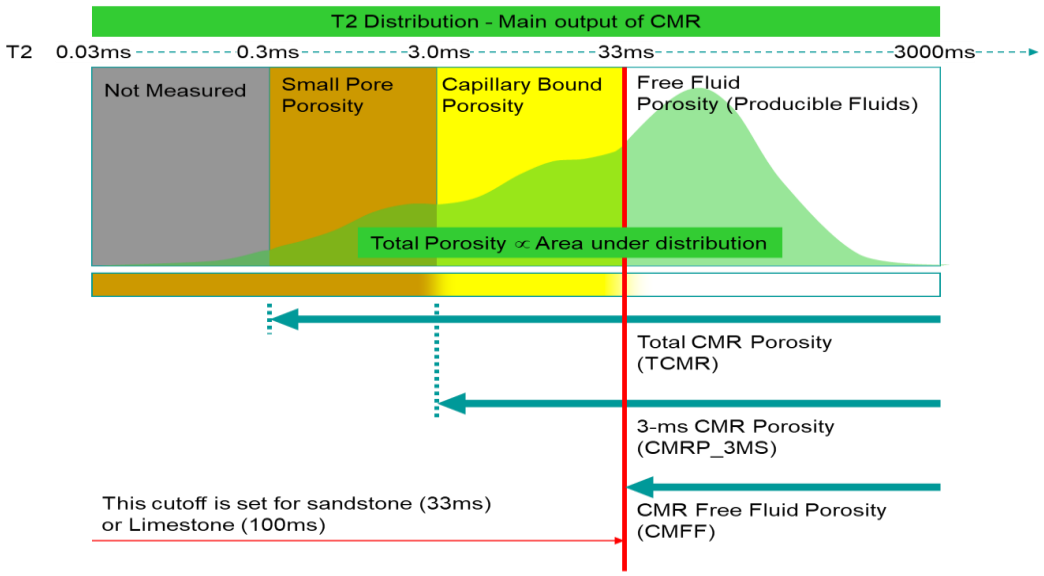

Fig. 4. T2 distribution curve from CMR. Cut-offs are used to get different bin porosities, and accordingly, Total porosity, Bound fluid volume, and Free fluid volumes are calculated. (Kameshwar Nath, 2003).

3. Results and interpretation

3.1 Lithological Components Identification

The identification of the matrix components and fluid typing is well defined through the Neutron-Density cross-plot. The Density -Neutron Cross plot shows that in Saffron-1 well reservoirs is characterized by a sandstone matrix with high porosity. The plotted points for this sand, as shown in (Figure-5), clearly indicate a cluster concentrated along the sandstone line in the 25% to 35% porosity range. The majority of these points, representing high-quality gas sand, have migrated to the northwest. This shift indicates the effect of the gas, as evidenced by a decrease in neutron porosity (average probability about 50% = 0.17) and a decrease in average density (approximately 2 g/cm³), as shown in the histograms.
Additionally, thin-bedded points are concentrated along the sandstone line in the 30% to 50% porosity range and have migrated eastward. This migration indicates the effect of clay, which increases neutron porosity (average probability about 50% = 0.44) and average density (approximately 2.1 g/cm³). (Fig.5).

For Saffron-2 well

Saffron reservoirs are characterized by a sandstone matrix with high porosity, as indicated by the plotted points in (Figure-6). The cluster of points is concentrated along the sandstone line in the 20% to 40% porosity range. Most of these points, representing high-quality gas sand, have migrated to the northwest, indicating the effect of the gas. This is evidenced by a decrease in neutron porosity (average probability about 50% = 0.18) and a decrease in average density (approximately 1.8 g/cm³).
Additionally, thin-bedded points are concentrated along the sandstone line in the 30% to 40% porosity range and have migrated to the east. This migration indicates the effect of clay, which increases neutron porosity (average probability about 50% = 0.35) and average density (approximately 2 g/cm³). (Fig.6).

For Saffron-Dlb well

A sandstone matrix with high porosity characterizes reservoirs. The plotted points for this sand (Figure-7) clearly indicate a cluster concentrated along the sandstone line within the 20% to 35% porosity range. Most of these points, representing high-quality gas sand (marked by red dots), have migrated to the northwest. This migration signifies the effect of gas, as evidenced by a decrease in neutron porosity (average probability about 50% = 0.15) and a decrease in average density (approximately 1.9 g/cm³), as shown in the histograms.
Additionally, the water sand points (marked by blue dots) have migrated to the northeast, indicating the effect of water sand. This is demonstrated by the neutron porosity (average probability about 50% = 0.3) and the average density (approximately 2.2 g/cm³), as depicted in the histograms. (Fig.7).

For Saffron-Dn well

A sandstone matrix with high porosity characterizes reservoirs. The plotted points for this sand (Figure-8) indicate a cluster concentrated along the sandstone line within the 25% to 35% porosity range. Most of these good-quality gas sand points have migrated to the northwest. This migration indicates the effect of the gas, as evidenced by a decrease in neutron porosity (average probability about 50% = 0.15) and a decrease in average density (approximately 1.85 g/cm³). (Fig.8).

3.2 Well Log Analysis

The input data and output results of Saffron reservoirs in the four wells are drawn in (Figs.9, 10, 11&12).The lithology for Saffron reservoirs is primarily sandstone with shale interbeds.
The average porosity calculated by conventional tools ranges from 18% to 27%, while CMR values range from 18% to 30%. Water saturation calculated by conventional tools ranges from 25% to 68%,

while CMR values range from 20% to 77%. (Table 1 and 2).

3.3 Reservoir Pressure and Connectivity

It can be concluded that in the next points and Saffron Field pressure data plot. (fig.13)

Northern Saffron Field Wells:

Wells such as Saffron-1, Saffron-2, and others in the northern part of the Saffron Field exhibit the same pressure trend with gas gradient = 0.06 psi/ft and share a regional water contact, detected in Saffron-1 through wire line logs and pressure data at 2176m TVDss.

Saffron-Dn Well:

Drilled in 2006 in the west of the Saffron Field, Saffron-Dn was analyzed after approximately four years of production (since 2002). The well showed a depletion of around 190 psi from the initial pressure, confirming that Channel C is connected to the other reservoirs.

Saffron-Dlb Well:

Drilled in 2008 in the southern part of the Saffron Field, Saffron-Dlb targeted Channel A-South, which is separated from the northern Saffron Field by a gas chimney. After around six years of production, the well maintained its initial pressure, approximately 50 psi higher than the initial pressure found in Saffron-1. Additionally, a different regional water contact was found at 1790m TVDss, confirming that Channel A-South is completely isolated and not connected to the rest of the channels.

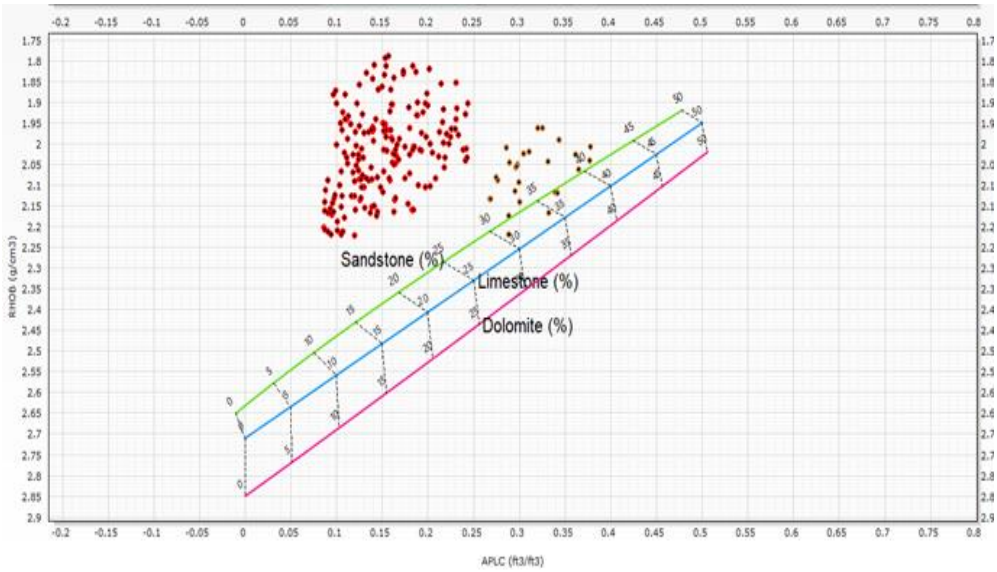

Fig. 5. N-D cross plot for Saffron-1.

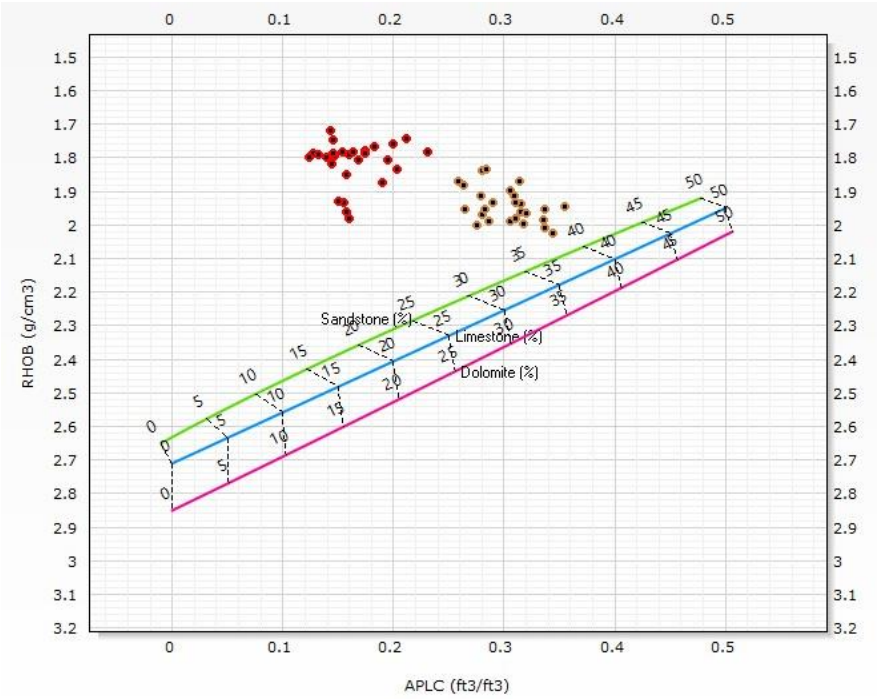

Fig. 6. N-D cross plot for Saffron-2.

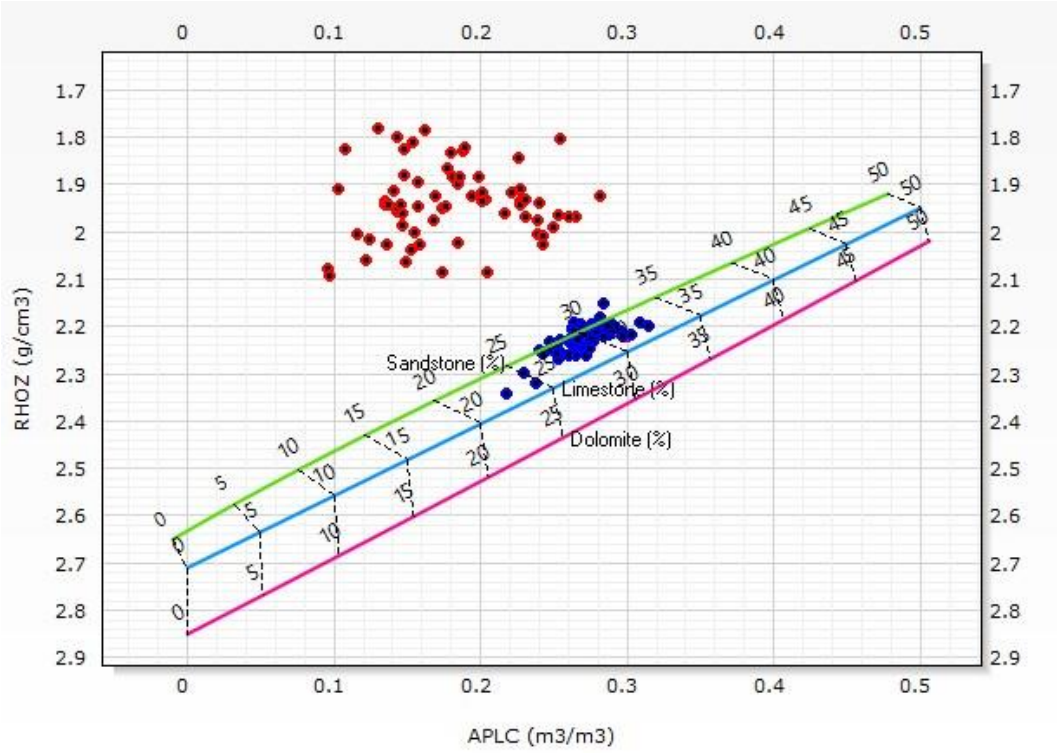

Fig. 7. N-D cross plot for Saffron-Dlb..

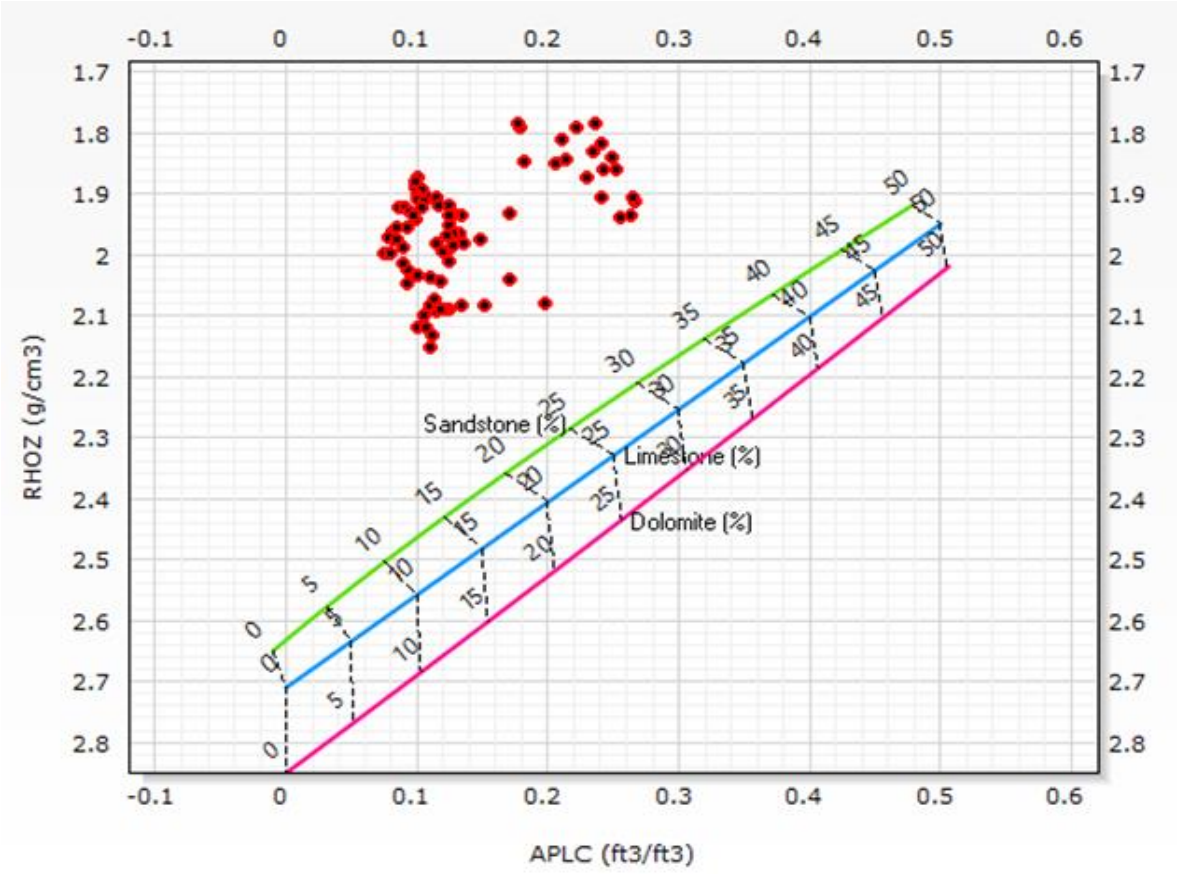

Fig. 8. N-D cross plot for Saffron-Dn.

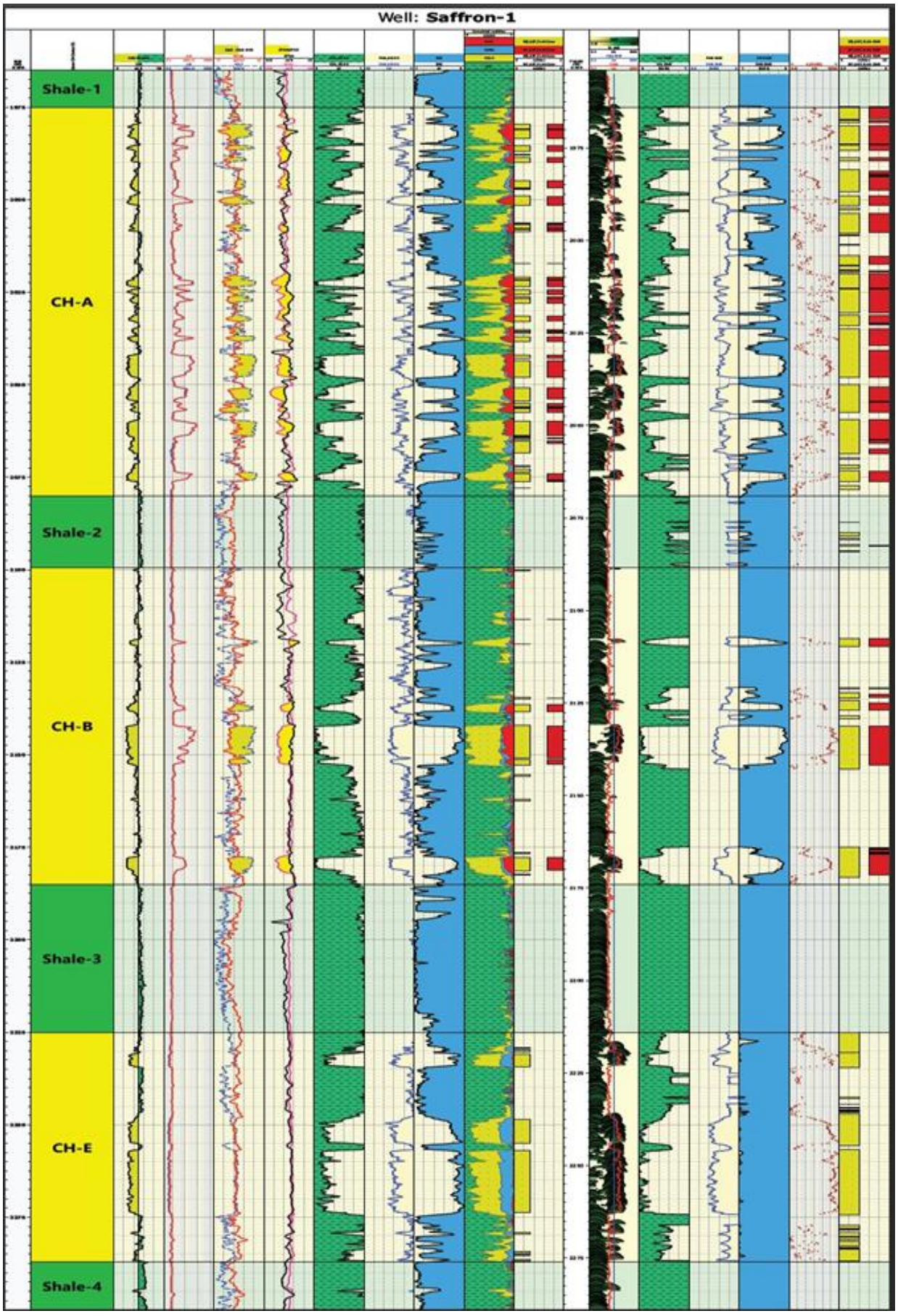

Fig. 9. Litho-Saturation Cross Plot for Saffron channels in Saffron-1 well.

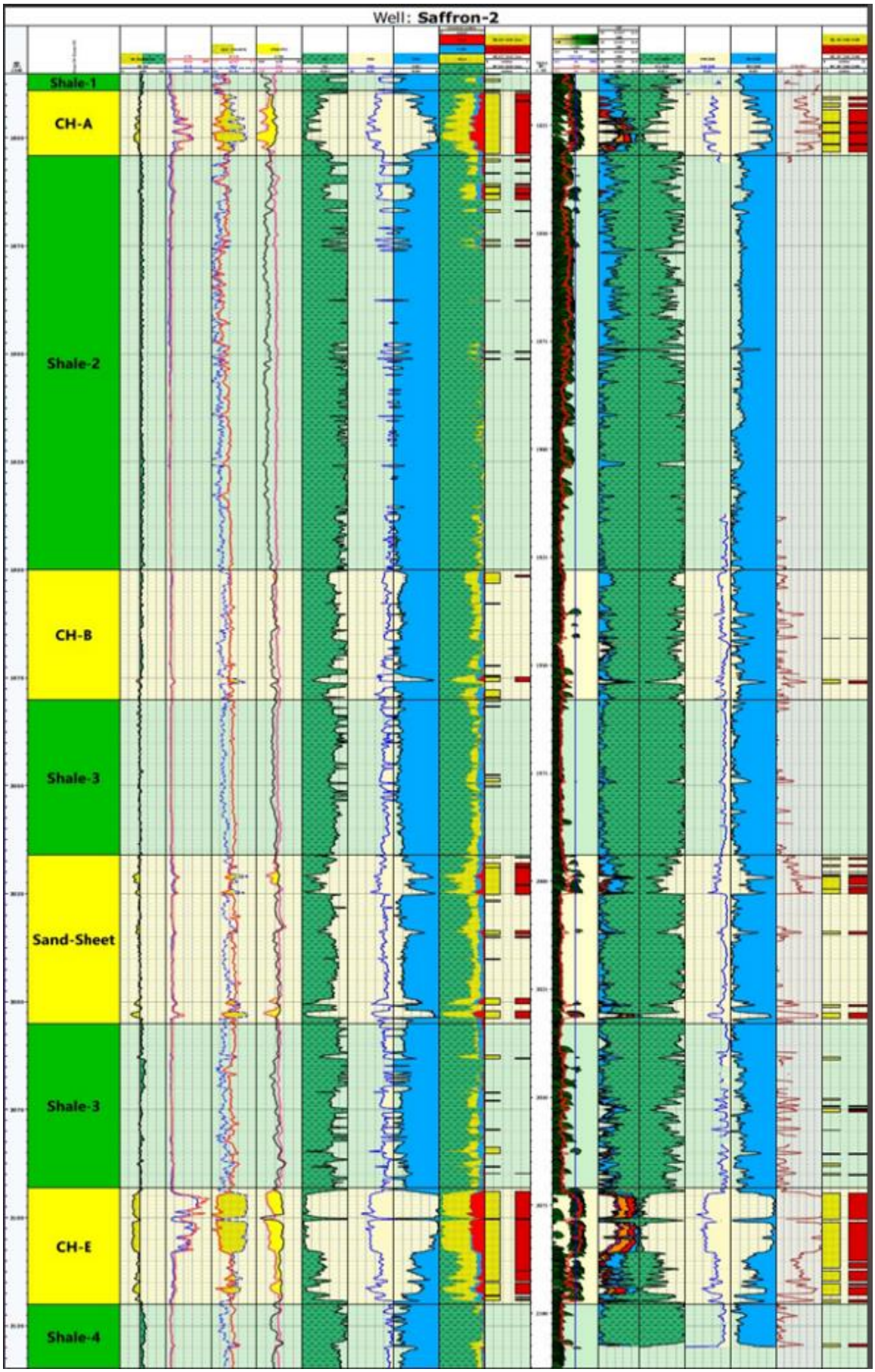

Fig. 10. Litho-Saturation Cross Plot for Saffron channels in Saffron-2 well.

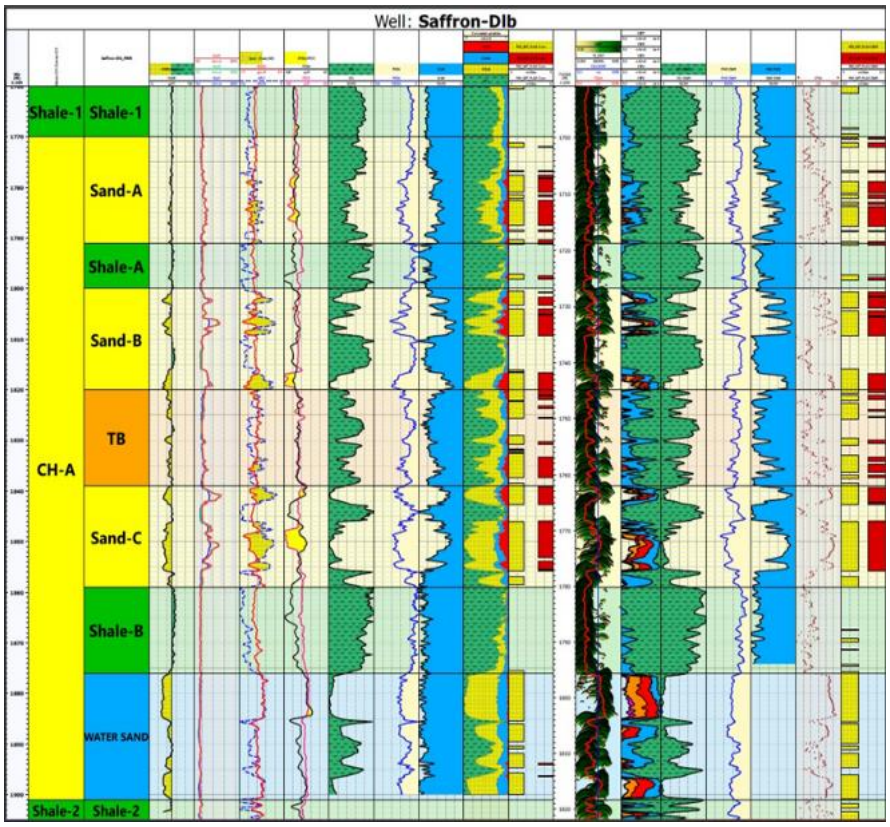

Fig. 11. Litho-Saturation Cross Plot for Saffron channels in Saffron-Dlb well.

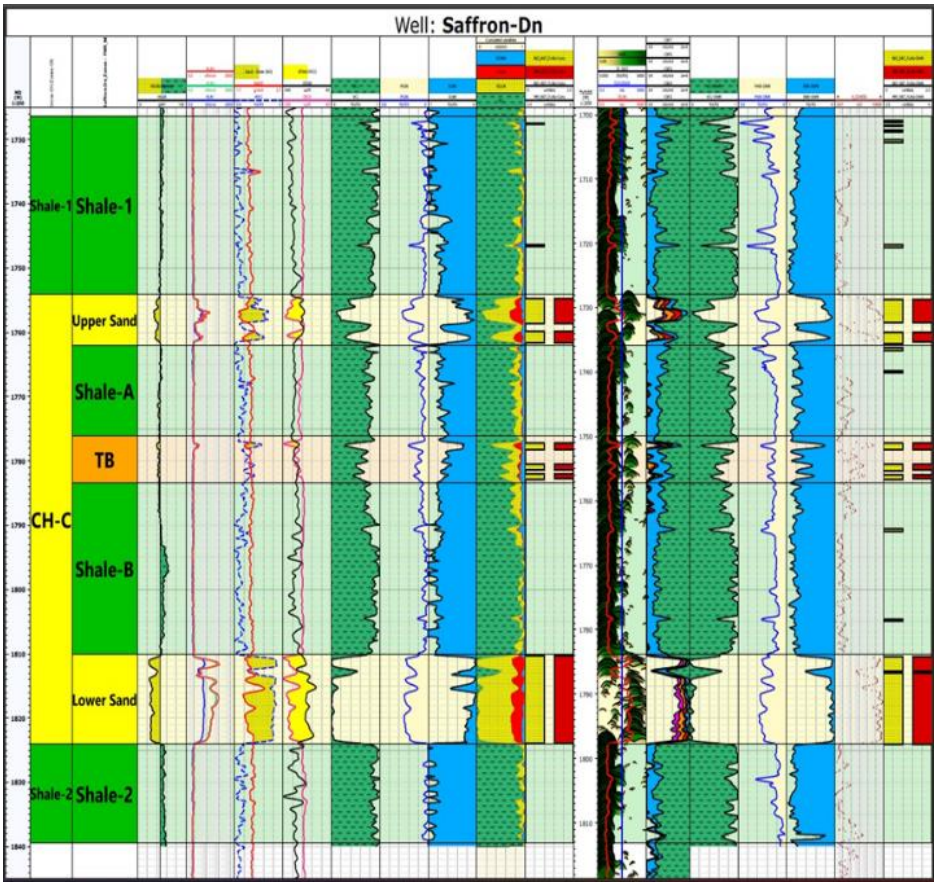

Fig. 12. Litho-Saturation Cross Plot for Saffron channels in Saffron-Dn well

Table 1. Conventional results for Saffron well.

Workflow Table Result MD												
Well	Zones	Flag Name	Top	Bottom	unit	Gross (m)	Net (m)	N/G	VSH (v/v)	PHIE (v/v)	SWE (v/v)	SHE (v/v)
Saffron-1	CH-A	RES	1975	2080	m	105	44.348	0.422	0.276	0.184	0.348	0.652
	CH-A	PAY	1975	2080	m	105	39.014	0.372	0.263	0.189	0.302	0.698
	CH-B	RES	2099	2185	m	85	18.288	0.214	0.165	0.237	0.345	0.655
	CH-B	PAY	2099	2185	m	85	15.392	0.18	0.106	0.256	0.294	0.706
	CH-E	RES	2225	2287	m	62	28.346	0.457	0.278	0.226	0.99	0.01
	CH-E	PAY	2225	2287	m	62	0	0				
Saffron-2	CH-A	RES	1839	1854	m	14.993	13.868	0.925	0.298	0.246	0.263	0.737
	CH-A	PAY	1839	1854	m	14.993	13.716	0.915	0.295	0.246	0.26	0.74
	CH-B	RES	1950	1980	m	30.004	5.977	0.199	0.512	0.155	0.712	0.288
	CH-B	PAY	1950	1980	m	30.004	1.219	0.041	0.367	0.164	0.371	0.629
	Sand-Sheet	RES	2016	2055	m	38.995	12.344	0.317	0.377	0.187	0.455	0.545
	Sand-Sheet	PAY	2016	2055	m	38.995	10.82	0.277	0.366	0.189	0.408	0.592
	CH-E	RES	2093	2120	m	26.996	24.384	0.903	0.219	0.25	0.212	0.788
	CH-E	PAY	2093	2120	m	26.996	23.317	0.864	0.21	0.253	0.195	0.805
Saffron-Dlb	CH-A	RES	1770	1901	m	130.999	74.219	0.567	0.283	0.218	0.637	0.363
	CH-A	PAY	1770	1901	m	130.999	40.843	0.312	0.276	0.236	0.477	0.523
	Sand-A	RES	1770	1791	m	20.998	11.336	0.54	0.455	0.199	0.59	0.41
	Sand-A	PAY	1770	1791	m	20.998	10.116	0.482	0.444	0.204	0.576	0.424
	Sand-B	RES	1800	1820	m	20	11.837	0.592	0.23	0.244	0.407	0.593
	Sand-B	PAY	1800	1820	m	20	10.313	0.516	0.208	0.255	0.373	0.627
	TB	RES	1820	1839	m	19	13.311	0.701	0.413	0.179	0.661	0.339
	TB	PAY	1820	1839	m	19	6.553	0.345	0.372	0.204	0.581	0.419
	Sand-C	RES	1839	1859	m	20	15.088	0.754	0.165	0.251	0.49	0.51
	Sand-C	PAY	1839	1859	m	20	12.497	0.625	0.133	0.266	0.442	0.558
	WATER SAND	RES	1876	1901	m	24.999	20.574	0.823	0.204	0.223	0.912	0.088
	WATER SAND	PAY	1876	1901	m	24.999	0	0				
Saffron-Dn	CH-C	RES	1754	1824	m	69.998	21.946	0.314	0.197	0.23	0.209	0.791
	CH-C	PAY	1754	1824	m	69.998	21.793	0.311	0.195	0.23	0.207	0.793
	Upper Sand	RES	1754	1762	m	8	5.639	0.705	0.328	0.229	0.247	0.753
	Upper Sand	PAY	1754	1762	m	8	5.639	0.705	0.328	0.229	0.247	0.753
	TB	RES	1776	1783	m	7.262	2.743	0.378	0.477	0.172	0.484	0.516
	TB	PAY	1776	1783	m	7.262	2.591	0.357	0.469	0.175	0.475	0.525
	Lower Sand	RES	1810	1824	m	14	13.564	0.969	0.086	0.242	0.155	0.845
	Lower Sand	PAY	1810	1824	m	14	13.564	0.969	0.086	0.242	0.155	0.845

Table 2. DMR results for Saffron well.

Workflow Table Result MD													
Well	Zones	Flag Name	Top	Bottom	unit	Gross (m)	Net (m)	N/G	VSH (v/v)	PHIE (v/v)	SWE (v/v)	SHE (v/v)	KTIM (mD)
Saffron-1	CH-A	RES	1975	2080	m	105	79.096	0.753	0.289	0.204	0.343	0.657	325.284
	CH-A	PAY	1975	2080	m	105	67.361	0.642	0.255	0.216	0.291	0.709	381.907
	CH-B	RES	2099	2185	m	85	27.28	0.319	0.212	0.212	0.291	0.709	721.497
	CH-B	PAY	2099	2185	m	85	22.555	0.264	0.154	0.23	0.229	0.771	872.588
	CH-E	RES	2225	2287	m	62	43.891	0.708	0.242	0.248	0.988	0.012	1698.29
	CH-E	PAY	2225	2287	m	62	0	0					
Saffron-2	CH-A	RES	1839	1854	m	14.993	10.516	0.701	0.292	0.277	0.266	0.734	2834.86
	CH-A	PAY	1839	1854	m	14.993	10.516	0.701	0.292	0.277	0.266	0.734	2834.86
	CH-B	RES	1950	1980	m	30.004	0.914	0.03	0.342	0.16	0.437	0.563	28.283
	CH-B	PAY	1950	1980	m	30.004	0.762	0.025	0.305	0.167	0.382	0.618	33.873
	Sand-Sheet	RES	2016	2055	m	38.995	7.468	0.192	0.382	0.189	0.459	0.541	494.736
	Sand-Sheet	PAY	2016	2055	m	38.995	7.01	0.18	0.377	0.19	0.439	0.561	526.808
	CH-E	RES	2093	2120	m	26.996	22.708	0.841	0.201	0.28	0.221	0.779	26119.8
	CH-E	PAY	2093	2120	m	26.996	21.793	0.807	0.188	0.284	0.207	0.793	27215.4
Saffron-Dlb	CH-A	RES	1770	1901	m	130.999	73.914	0.564	0.27	0.251	0.458	0.542	279.824
	CH-A	PAY	1770	1901	m	130.999	39.929	0.305	0.275	0.269	0.38	0.62	349.859
	Sand-A	RES	1770	1791	m	20.998	9.964	0.475	0.439	0.244	0.487	0.513	141.575
	Sand-A	PAY	1770	1791	m	20.998	9.812	0.467	0.437	0.245	0.484	0.516	143.334
	Sand-B	RES	1800	1820	m	20	12.142	0.607	0.272	0.264	0.335	0.665	468.672
	Sand-B	PAY	1800	1820	m	20	10.77	0.539	0.246	0.277	0.3	0.7	528.205
	TB	RES	1820	1839	m	19	11.025	0.58	0.379	0.225	0.681	0.319	48.337
	TB	PAY	1820	1839	m	19	5.182	0.273	0.298	0.253	0.542	0.458	97.265
	Sand-C	RES	1839	1859	m	20	15.632	0.782	0.18	0.278	0.378	0.622	402.73
	Sand-C	PAY	1839	1859	m	20	13.106	0.655	0.152	0.293	0.314	0.686	479.873
	WATER SAND	RES	1876	1901	m	24.999	21.488	0.86	0.157	0.254			310.02
	WATER SAND	PAY	1876	1901	m	24.999	0	0					
Saffron-Dn	CH-C	RES	1754	1824	m	69.998	22.81	0.326	0.23	0.277	0.223	0.777	1875.49
	CH-C	PAY	1754	1824	m	69.998	20.677	0.295	0.199	0.276	0.158	0.842	2068.98
	Upper Sand	RES	1754	1762	m	8	5.334	0.667	0.351	0.288	0.225	0.775	1712.85
	Upper Sand	PAY	1754	1762	m	8	5.029	0.629	0.34	0.291	0.195	0.805	1816.66
	TB	RES	1776	1783	m	7.262	2.743	0.378	0.486	0.236	0.462	0.538	101.718
	TB	PAY	1776	1783	m	7.262	2.438	0.336	0.476	0.242	0.435	0.565	114.172
	Lower Sand	RES	1810	1824	m	14	13.208	0.943	0.093	0.276	0.099	0.901	2526.2
	Lower Sand	PAY	1810	1824	m	14	13.208	0.943	0.093	0.276	0.099	0.901	2526.2

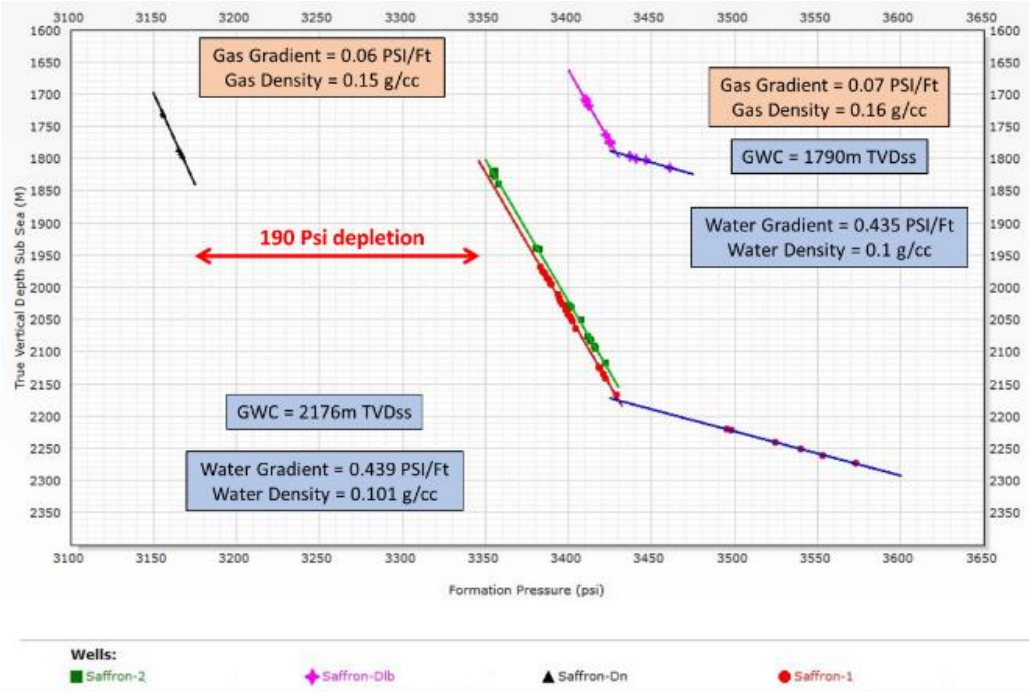

Fig. 13. Pressure Plot for Saffron field.

4. Summary and Conclusion

This study focuses on the reservoir Saffron reservoir's general geological setting and structural setup within the El Wastani Formation on the northwestern margin of the Nile Delta. Petrophysical analysis was conducted for the reservoir rocks in four wells to calculate parameters such as porosity, shale volume, permeability, water saturation, and hydrocarbon saturation. This analysis was used to develop litho-saturation cross-plots and lithologic identification cross-plots, along with examining lateral variations in lithology and saturation distributions. The study compared results from conventional tools with those from advanced tools (CMR) to select the most suitable model for the Saffron reservoir and examined reservoir connectivity and water levels through pressure-depth plots.

The study can be summarized as follows

Well Logging Analysis

Well logging analysis was conducted for the Saffron reservoir in the four selected wells, determining fluid resistivities (Rm, Rmf, and Rw) at formation temperatures. Water resistivity (Rw) was determined through water sample measurement and resistivity in clean water-bearing zones. Uninvaded zone resistivities (Rt) were calculated from available resistivity logs using Techlog-v.2019 petrophysics software. The Volume of shale (Vsh) was calculated using GR and resistivity methods as single indicators and neutron-density methods as double indicators.

Corrected rock porosity (Φ) was calculated using:

-Conventional tools: Sonic, Density, Neutron logs

-Advanced tools: CMR tool

The fluid saturations were determined for both clean and shaly zones, with Archie's equation applied to clean zones and the Indonesian model applied to shaly zones. Results were compared with water saturation calculated from the CMR tool, and the closest results to CMR were found in the Indonesian model.

Permeability Determination

The NMR data is used extensively to compute permeability this is because there is a direct correlation between permeability and the following Parameters:

-Surface area/Pore volume ratio(S/V)

-Pore throat diameter and hence pore size

-Porosity:

So that in this study Timur-Coates model is used to calculate permeability as it is the best method for gas reservoirs.

Lithological and Mineralogical Evaluation

The lithology and mineralogy of the Saffron reservoir rock were studied using various cross-

plots (density-neutron, Th-K, PE-K, and PE-Th/K cross-plots). These plots indicated that the reservoir rock is primarily composed of sandstone matrix with shale interbeds, consisting mainly of mixed layer clay, montmorillonite, illite, and moderate percentages of mica and glauconite.

Hydrocarbon Potentialities

The vertical and horizontal distributions of hydrocarbon occurrences were exhibited through litho-saturation cross-plots of the four evaluated wells.

A.Vertical Distribution of Petrophysical Parameters

The litho-saturation cross-plots showed that the Wastani Formation mainly consists of claystone with streaks of sandstone and siltstone, while the Saffron reservoir is primarily sandstone with shale interbeds.

The average porosity calculated by conventional tools ranges from 18% to 27%, while CMR values range from 18% to 30%. Water saturation calculated by conventional tools ranges from 25% to 68%, while CMR values range from 20% to 77%.

B. Reservoir Pressure and Connectivity:

MDT pressure data was collected from four wells in various compartments of the Saffron Field. The data analysis indicated that the Saffron-Dlb well in the southern area is modeled as a separate compartment, while the rest of the field is treated as one interconnected reservoir, with a slight pressure difference between the south and north.

The free water level was identified at 2176m TVDss in Saffron-1 and at 1790m TVDss in Saffron-Dlb.

5. Recommendations

It is advisable to utilize the Density–Magnetic Resonance (DMR) method to calculate gas-corrected total formation porosity, as it provides more precise reservoir volume estimates. Additionally, using gas-corrected total porosity in conjunction with deep-reading resistivity tools allows for the computation of more accurate formation gas saturations.

Moreover, it is recommended to apply the Indonesian model to calculate water saturation in this reservoir. For permeability calculations, the Timur-Coates model is suggested due to its effectiveness in gas reservoirs.

For further field development it is recommended according to all the previous analysis (MDT-litho saturation cross plots) to:

1-Drill a new well in the southern Part around Saffron-Dlb: This well aims to delineate Channel A in the southern part of the Saffron Field.

2-Drill another well in the western part around the Saffron-Dn area: This well targets the delineation of channel C

6. References

Abdel Aal A, Price RJ, Vaitl JD, Shrallow JA (1994). Tectonic evolution of the Nile Delta, its impact on sedimentation and hydrocarbon potential. In: Proceedings of the 12th Petroleum Conference of EGPC, Cairo, pp. 19-34. Cairo: Egyptian General Petroleum Corporation.

Abdel Aal A, Shrallow JA, Nada H, Shaarawy O (1996). Geological evolution of the Nile Delta, Egypt, using REGL, Regional seismic line interpretation. In: Proceedings of the 13th Exploration and Production Conference EGPC, Cairo, Egypt, pp. 242-255. Cairo: Egyptian General Petroleum Corporation.

Abu El Ata AS, El Gendy NH, El Nikhely AH, Raslan S, El Oribi M, Barakat MK (2023). Seismic characteristics and AVO response for non-uniform Miocene reservoirs in offshore eastern Mediterranean region, Egypt. In: Scientific Reports, vol. 13, article pp. 88-97. https://doi.org/10.1038/s41598-023-40838-3.

Barakat GM (1982). General review of the petroliferous provinces of Egypt with special emphasis on their geological setting and oil potentialities. In: Research projection resources development and policy in Egypt: Petroleum and natural gas, Cairo University-Massachusetts Institute of Technology, pp. 34-56. Cairo: Massachusetts Institute of Technology.

Barakat M, Dominik W (2010). Seismic studies on the Messinian rocks in the Onshore Nile Delta, Egypt. In: 72nd European Association of Geoscientists and Engineers Conference and Exhibition, cp-161-00770. https://doi.org/10.3997/2214-4609.201401362.

Coates GR, Xiao L.Z., Prammer MG (1998). NMR logging principles and applications. In: Gulf Publishing Company, Houston, pp. 42-78.

El-Gendy NH, Mabrouk WM, Waziry MA, Dodd TJ, Abdalla FA, Alexakis DE, Barakat MK (2023). An integrated approach for saturation modeling using hydraulic flow units: Examples from the Upper Messinian Reservoir. In: Water, vol. 15(24), article 4204, pp. 4-12. https://doi.org/10.3390/w15244204.

El-Gendy NH, El-Nikhely AH, Zakaria AH, Hellish HM, Nabawy BS, Barakat MK (2023). Pre-stack imaging

for the Messinian sub-salt sequences in the Levantine Basin of the East Mediterranean: A case study, offshore Lebanon. In: The Iraqi Geological Journal, pp. 1-18.

Hassoun TH, Zainalabedin K (1997). Hydrocarbon detection in low contrast resistivity pay zones, capillary pressure and ROS determination with NMR logging in Saudi Arabia. In: SPE Paper 37770, presented at the 10th Middle East Oil Show (MEOS), Bahrain, pp. 15-18.

Freedman R (1997). Gas-corrected porosity from density-porosity and CMR measurements. In: How to use borehole nuclear magnetic resonance: Oilfield Review, vol. 9, no. 2, p. 54.

Hamouda AZ, El-Gendy N, El-Gharabawy S, Salah M, Barakat MK (2023). Marine geophysical surveys and interpretations on the ancient Eunostos harbor area, Mediterranean coast, Egypt. In: Egyptian Journal of Petroleum, vol. 32, issue 1, pp. 47-55.

Kirschbaum MA, Schenk C, Charpentier R, Klett T, Brownfield M, Pitman J, Cook T, Tennyson M (2010). Assessment of undiscovered oil and gas resources of the Nile Delta Basin Province, eastern Mediterranean. U.S. Geological Survey Fact Sheet 2010-3027.

Kleinberg RL, Vinegar HJ (1996). NMR properties of reservoir fluids. In: The Log Analyst, November-December, pp. 20-32.

Kameshwar Nath M, Haseeb M, Katiyar GC (2003). Successful application of CMR tool in identifying pay zones in complex lithology: Case study from Ahmedabad field, Cambay Basin, India. In: 10th Biennial International Conference & Exposition, SPG India, Vadodara.

Mao Z.Q., Zhang C., Xiao L. (2010). A NMR-based porosity calculation method for low porosity and low permeability gas reservoir. In: Oil Geophys Prospect, Volume 45(1): pp. 105-109.

Prammer MG, Mardon D, Coates GR, Miller MN (1995). Lithology-independent gas detection by gradient-NMR logging. In: SPE Paper 30562, Transactions of the Society of Petroleum Engineers Annual Technical Conference and Exhibition.

Reda M, El-Gendy NH, Raef A, Elmashaly MM, AlArifi N, Barakat MK (2024). Advancing Neogene-Quaternary reservoir characterization in offshore Nile Delta, Egypt: high-resolution seismic insights and 3D modeling for new prospect identification. In: Environmental Earth Sciences, vol. 83(20), article 581. https://doi.org/10.1007/s12665-024-10632-5.

Schlumberger Well Services, Inc. (1972). Log interpretation/charts. Houston.

Schlumberger (1975). A guide to wellsite interpretation of the Gulf Coast. Schlumberger Well Services, Houston, 85.

Schlumberger (1984). Egypt Well Evaluation Conference (WEC), Cairo, Egypt. Smith CM. pp. 47-54.

Schlumberger (1989). Log interpretation principles applications. Schlumberger Well Services.

Timur A (1969). Effective porosity and permeability of sandstones investigated through nuclear magnetic principles. In: The Log Analyst, vol. 10(1), p. 3.

دراسات بتروفيزيقية لخزانات الرمال الطينية في حقل الزعفران، دلتا النيل، مصر

أسامة سعيد مصيلحي[١]، وعبدالمقتدر عبدالعزيز السيد[٢]، وأمير ماهر سيد لالا[٢]

[١]شركة رشيد للبترول، القاهرة، جمهورية مصر العربية

[٢]قسم الجيوفيزياء، كلية العلوم، جامعة عين شمس، القاهرة، جمهورية مصر العربية

حقل الزعفران الغازي، الذي يقع ضمن امتياز غرب دلتا البحر العميق (WDDM) على الحافة الشمالية الغربية لدلتا النيل. يتم استخراج الهيدروكربونات في هذا الحقل من خزانات رمال الزعفران. تم حفر العديد من الآبار التي اخترقت هذه الخزانات. تهدف التقييمات البتروفيزيقية ، التي أجريت باستخدام بيانات سجلات الآبار، إلى تحديد الخزانات المحتوية على الهيدروكربونات وفحص خصائص الخزان استنادًا إلى بيانات من أربعة آبار. تعتمد هذه الدراسة على حزم البرمجيات Techlog–v.2019 من شركة شلمبرجير في تحليلاتها وقد وفرت الآبار الأربعة بيانات كافية للتحليل المفصل، مما سمح بتقييم بعض المعايير البتروفيزيقية مثل حجم الطين (Vsh)، المسامية الكلية (PHT)، المسامية الفعالة (PHE)، تشبع الماء (Sw)، تشبع الهيدروكربون (Sh)، وسمك الخزان الصافي إلى الإجمالي. تم استخدام أدوات السجلات التقليدية وأدوات CMR المتقدمة في هذه الدراسة، مع المقارنة بين التقنيات التقليدية والمتقدمة.